Journal of ELECTRONIC MATERIALS
https://doi.org/10.1007/s11664-018-6822-4

Design Optimization of an Anisotropic Magnetoresistance Sensor for Detection of Magnetic Nanoparticles

L.K. QUYNH,[1,2,4] B.D. TU,[1] C.V. ANH,[1] N.H. DUC,[1] A.T. PHUNG,[3] T.T. DUNG,[2] and D.T. HUONG GIANG[1,5]

1.—University of Engineering and Technology, Vietnam National University, Hanoi, Vietnam. 2.—Faculty of Physics, Ha Noi Pedagogical University 2, Hanoi, Vietnam. 3.—Hanoi University of Science and Technology, Hanoi, Vietnam. 4.—e-mail: quynhlk@gmail.com. 5.—e-mail: giangdth@vnu.edu.vn

Recent studies have shown that the magnetic field sensitivity of an anisotropic magnetoresistance (AMR) sensor using a single-layer $Ni_{80}Fe_{20}$ thin film can be considerably improved by increasing the shape anisotropy of the film. In this work, an effective approach for improving the sensitivity and reducing the magnetic coercive field as well as the thermal noise contribution in an AMR Wheatstone bridge sensor is proposed by combining multiple resistors in the series–parallel combination circuits. Four different AMR sensor designs, consisting of a single resistor, three and five resistors in series and six resistors in series–parallel connection, were fabricated by using Ta (10 nm)/$Ni_{80}Fe_{20}$ (5 nm)/Ta (10 nm) films grown on thermally oxidized Si substrates under the presence and the absence of a biasing magnetic field (900 Oe). The results showed that the sensors based on series–parallel combination gain a magnetic sensitivity (S_H) 1.72 times higher than that of the sensor based on the series connection. This optimized sensor has improved the capacity of detecting various concentrations of magnetic nanoparticles with a detection limit of magnetic moments estimated to be about 0.56 μemu.

Key words: Anisotropic magnetoresistance, Wheatstone bridge, magnetic sensor, magnetic nanoparticle detection

INTRODUCTION

High-performance Wheatstone bridge magnetic sensors based on the anisotropic magnetoresistive (AMR) effect have been developed with excellent features, such as high sensitivity, reduction of thermal noise and simple structure.[1,2] They have been applied as sensors for detecting low-magnetic, stray fields of magnetic nanoparticles.[2–4] Figure 1 shows a typical AMR sensor composed of four AMR bridge arms (R_1, R_2, R_3 and R_4) of NiFe (permalloy) film. In an applied magnetic field, the change of angle between the magnetization and current flow directions in the pair of resistors R_1 and R_3 is different than in R_2 and R_4, which causes a different relative change in resistance (ΔR). For a given voltage input (V_{in}), the sensor's voltage response ΔV_{out} related to the resistance change in a balanced bridge is simplified to:

$$\Delta V_{out} = \frac{r}{(1+r)^2}\left(\frac{\Delta R_1}{R_1} - \frac{\Delta R_2}{R_2} + \frac{\Delta R_3}{R_3} - \frac{\Delta R_4}{R_4}\right)V_{in} \quad (1)$$

where r is defined by

$$\frac{1}{r} = \frac{R_1}{R_2} = \frac{R_4}{R_3} \quad (2)$$

The sensor's voltage response that can be improved by increasing the relative resistance change $\Delta R/R$ in R_1 and R_3 and by decreasing that in R_2 and R_4. In a recent work, we have shown that the performance of an AMR Wheatstone bridge sensor can be strongly enhanced thanks to the induced uniaxial

(Received September 21, 2018; accepted November 16, 2018)

Published online: 29 November 2018

anisotropy. This has been achieved by using a pair of bar magnets to produce a substantially uniform magnetic field aligned along the bridge arms R_1 and R_3 during the sputtering process. In addition, shape magnetic anisotropy is enhanced by optimizing the length, width and thickness of the $Ni_{80}Fe_{20}$ film.[2] Due to shape anisotropy, the magnetic moments are more preferably aligned along the pinned direction in R_1 and R_3 (parallel to the length) than in R_2 and R_4 (perpendicular to the length). When a magnetic field is applied along the hard axis, the resistance tends to increase in R_1 and R_3 and decrease in R_2 and R_4 due to the magnetization reversal. As a result, the sensor's sensitivity was remarkably increased as reported in Ref [2]. For low-magnetic-field sensing, the AMR sensor based on an uniaxial single-layer NiFe thin film was used in our work reported in Ref. [5], which considered the planar Hall effect (PHE)-based sensor that uses the pinned conventional NiFe/IrMn bilayer thin films. Indeed, it has been reported that by using the Wheatstone bridge design instead of a traditional cross-shaped Hall geometry, the sensor output increases by a factor of 100.[6] It was worth mentioning that the sensor geometry was patterned with several resistor bars (n) connected in series, but the connection between the resistor bars was a magnetic material.

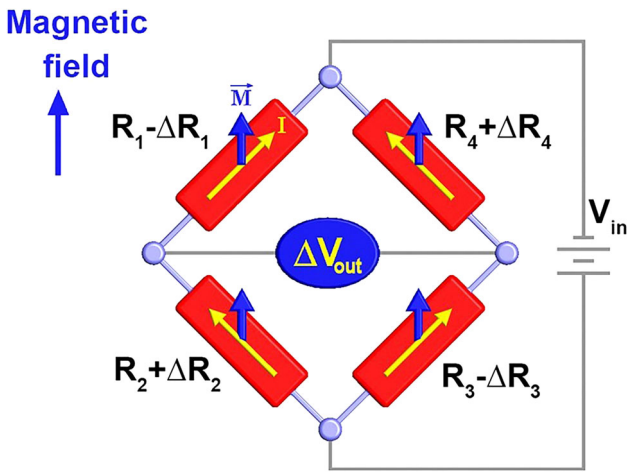

Fig. 1. Schematic diagram of a typical AMR Wheatstone bridge.

A recent study by Doescher et al.[7] has shown that the coercivity of the AMR sensor can be further reduced by designing a Wheatstone bridge consisting of a plurality of resistance elements such that demagnetization fields build up in the surroundings of the resistor elements. To increase the resistance change contribution in the AMR sensor, and so to increase sensitivity of the sensor, a higher number of magnetic resistors were added in each branch of the bridge design. However, this leads to the increase in the total resistance of the bridge and gives rise to Johnson noise resulting from the random thermal motion of electrons:[8]

$$S_J\left[V^2\mathrm{Hz}^{-1}\right] = 4k_BTR \tag{3}$$

where k_B is Boltzmann's constant, T is the temperature and R is the bridge resistance. This also limits the AMR bridge sensor from achieving an improved signal-to-noise ratio.

In the present work, we show how the Johnson contribution limitation of such an AMR sensor can be overcome. We achieve this by using a non-magnetic connecting material between resistor elements combined with optimal designs that consist of multiple resistors in a series–parallel combination. This design results in further enhancement of the sensor signal output voltage as well as the reduction of the coercive field. Thanks to their simple structure, design and cost-effective production, the custom-designed sensor is reliable for the detection of magnetic nanoparticles at various concentrations, which may find important applications in nanomedicine.[9–14]

EXPERIMENTAL

Different types of sensor structures were fabricated by combining magnetron sputtering and lithography techniques. The film deposition was performed with a commercial magnetron sputtering system (Model ATC 2000) using an NiFe target. The magnetic anisotropy of NiFe layers with easy axis anisotropy were formed by applying a magnetic field (denoted as H_{pinned}) of approximately 900 Oe during the sputtering process. The thickness of the NiFe is approximately 5 nm. To prevent

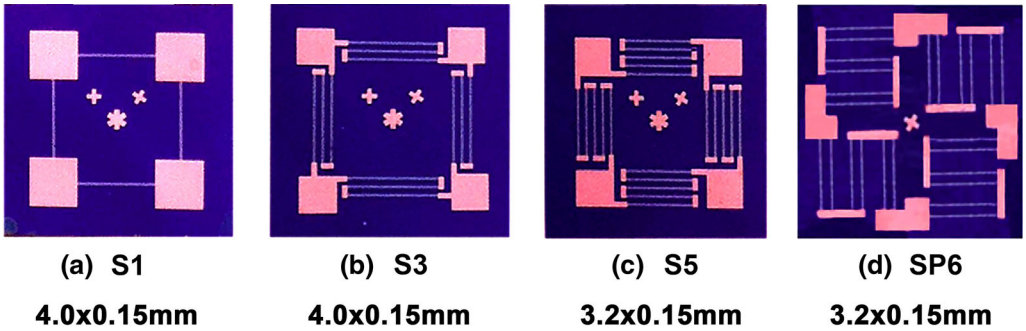

Fig. 2. Optical microscopy images of different fabricated AMR sensors: single resistor (a), three and five resistors connected in series (b, c) and six resistors in series–parallel combination (d).

oxidation, a 10-nm Ta layer is deposited on top of the NiFe. Two photolithography steps were carried out using lift-off and opening contact windows for a thick Cu contact layer. Figure 2 shows an optical microscopy image of the fabricated AMR sensor. The four branches were arranged within a square of 12 × 12 cm^2. To improve the influence of junctions between segments of multiple bars in the AMR Wheatstone bridge, sensors using Cu (nonmagnetic) and NiFe (magnetic) junctions have been fabricated with the same geometry. In this design, one branch of the Wheatstone bridge consisted of six parallel 1 mm × 10-mm bars connected in series. The space between bars was kept at 1 mm. For optimizing the Wheatstone bridge design, four types of AMR sensors were fabricated consisting of a single resistor (named S1, Fig. 2a), three and five resistors connected in series (named S3 and S5, Fig. 2b and c) and six resistors combined in series–parallel (named SP6, Fig. 2d). The width of all the elements was 0.15 mm and the length was 4.0 mm for S1 (Fig. 2a) and S3 (Fig. 2-b), and 3.2 mm for S5 (Fig. 2c) and SP6 (Fig. 2d). The length-to-width aspect ratios were 26.67 and 21.33, respectively. The center-to-center element separation was fixed at 350 μm. The sensors were wire-bonded to a printed circuit board for magnetoresistance (MR) characterization. The four-terminal direct current (DC) measurements were performed using the Keithley 6220 DC Precision Current Source in which a current was applied to two opposite corners of the bridge. The remaining two contacts were used to measure the DC voltage, V_{out}, response of the bridge as a function the applied magnetic field (H_{app}) in the plane of the film and perpendicular to the H_{pinned} direction using a Keithley 2400 multimeter. The MR effect was measured at room temperature in a homogenous magnetic field created by a pair of Helmholtz coils (Lake Shore Model MH-2.5) with a range of −30 to 30 Oe.

RESULTS AND DISCUSSION

Figure 3 shows the normalized magnetization versus applied magnetic field in a 10 × 10-mm^2 square and 5-nm thin film. The magnetic field was applied in-plane, along the easy and hard axes. In Fig. 3a, there is almost no difference in the magnetic hysteresis loops for films sputtered in the absence of a magnetic field (H_{pinned} = 0 Oe), which indicates that the NiFe film is in-plane isotropic. When H_{pinned} = 900 Oe (Fig. 3b), the film exhibited strong uniaxial anisotropy. In this case, the anisotropy field (H_k) was determined from magnetization curves to be approximately 10 Oe. The uniaxial anisotropy energy density ($K = H_k M_s/2$) was calculated to be 3.9 × 10^4 erg/cm^3, which is much higher than in bulk films (1.44 × 10^3 erg/cm^3).[8]

Figure 4a displays a schematic of a six-resistor set up of NiFe bars connected in series by either Cu or NiFe, which would act as an R_1 or R_3 branch in a Wheatstone bridge sensor. Figure 4b shows the relative change in MR as a function of external magnetic field applied along the hard axis in NiFe bars with Cu and NiFe connections, respectively. The results show that the MR ratio of 0.25% in the sample with the Cu connector is 1.5 times higher than that value of 0.167% in the sample with an NiFe connector.

To verify this phenomenon, the Maxwell 2D software (Ansys, Canonsburg, PA, USA) was utilized for magnetic simulation using the finite element method. Here, the measured magnetization B-H curve of a 5-nm NiFe thin film was used to model the magnetic flux density distributed on each magnetic bar. The results shown in Fig. 5a and b reveal that the magnetic flux distributes homogeneously in a wider region in a sample with a Cu junction than an NiFe junction. For center bars, this range in the sample with an NiFe junction was estimated to be 1.3 times higher than that in the sample with a Cu junction. This ratio agrees well

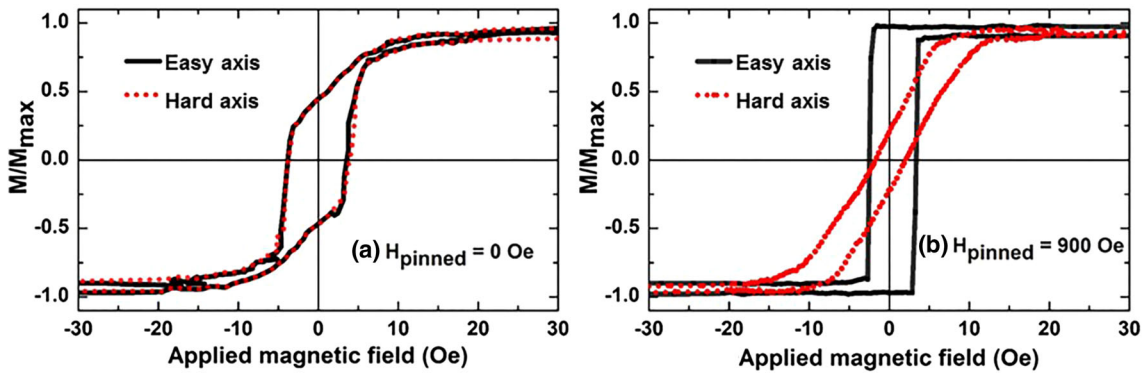

Fig. 3. Hysteresis loops of NiFe film grown with (a) and without an (b) applied magnetic field of 900 Oe (H_{pinned}) during the sputtering process. The magnetic field was applied in-plane, along the easy axis (solid line) and hard axis (dashed line).

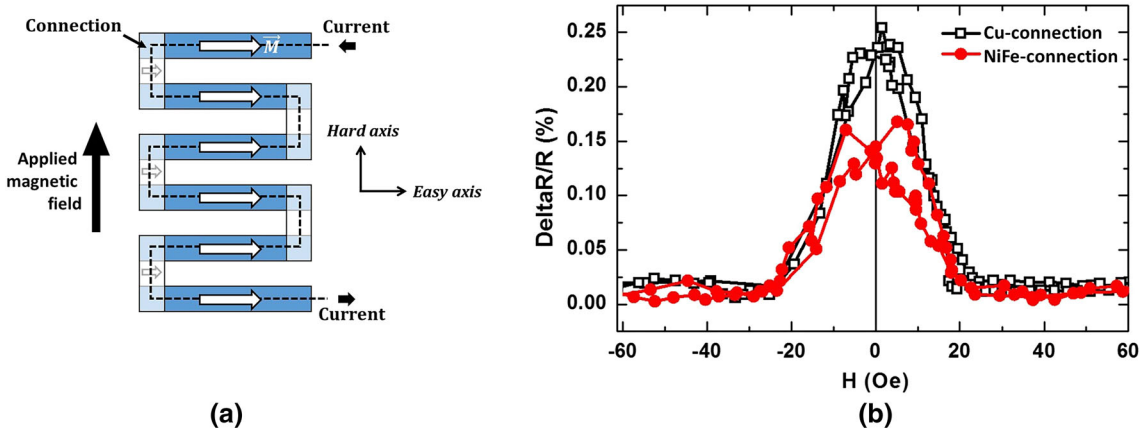

Fig. 4. Schematic of NiFe bars connected in series with Cu and NiFe connections (a) and the relative magnetoresistance change versus applied magnetic field (b).

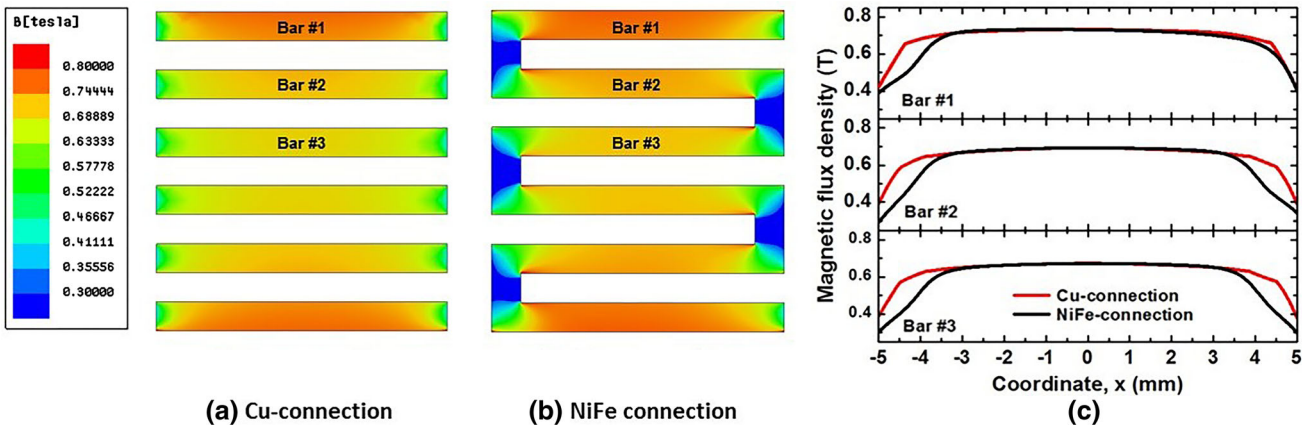

Fig. 5. Magnetic flux density distribution on the multi-bar sample with a non-magnetic (a) and a magnetic junction (b) and the extracted data plotted at the center line along the length of different bars (c).

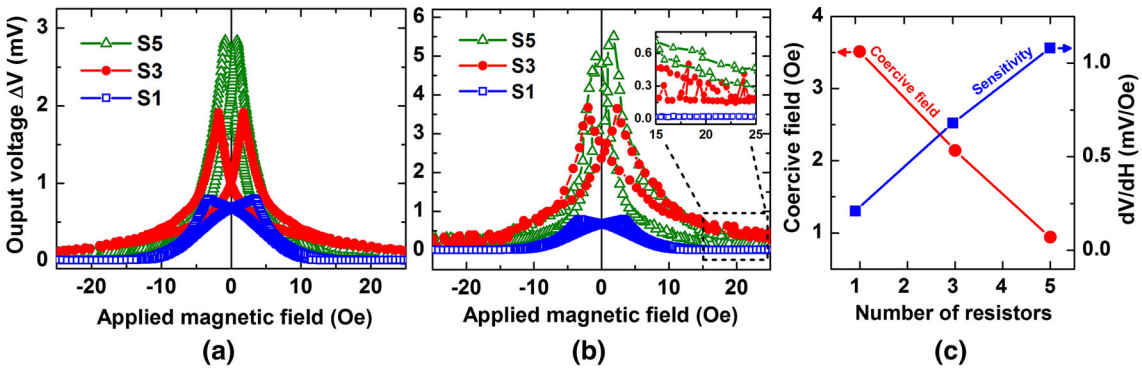

Fig. 6. Magnetic field dependence of output voltage response at a current of 0.1 mA (a) and 0.2 mA (b). Coercive magnetic field and sensitivity, dV/dH, (c) measured in AMR bridge sensors with one, three and five resistors connected in series (denoted as S1, S3 and S5, respectively).

with the relative decrease of the MR ratio shown in Fig. 4b. The difference can be attributed to the demagnetization magnetic field (H_d) contribution. Without an external magnetic field, the total magnetic flux is given as follows:

$$\vec{B} = \mu_0\left(\overrightarrow{M} + \vec{H}_d\right). \quad (4)$$

The weakening magnetic flux at the two ends of the NiFe bar in the case of the NiFe connection is

Table I. The coercive field (H_C), resistance (R), output voltage (ΔV), magnetic field derivative of the voltage (dV/dH) and the magnetic field sensitivity (S_H) measured at current of 0.1 mA on different sensors

Sensor	H_C (Oe)	R (kΩ)	ΔV (mV)	dV/dH (mV/Oe)	S_H (mV/V/Oe)
S1	3.51	1.20	0.80	0.21	1.75
S3	2.14	3.64	1.91	0.68	1.87
S5	0.94	6.16	2.85	1.08	1.75
SP6	1.70	1.80	1.18	0.55	3.06

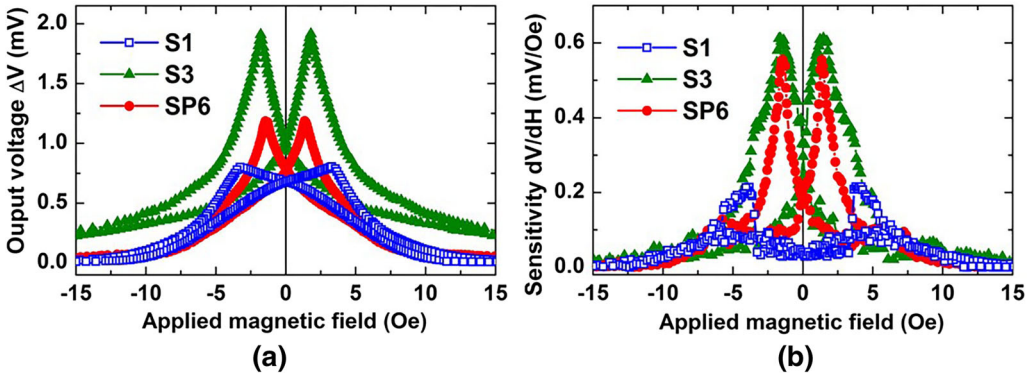

Fig. 7. Magnetic field dependence of magnetoresistance (a) and sensitivity (b) measured in AMR bridge sensors of one and three (S1 and S3) resistors in series and six resistors in combined series–parallel (SP6).

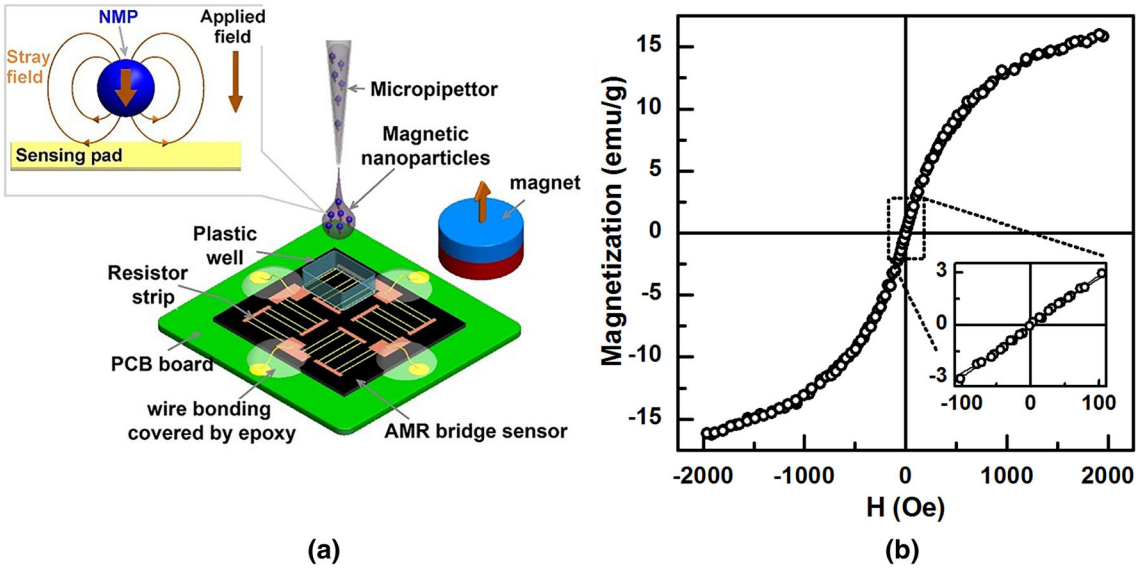

Fig. 8. Schematic of magnetic nanoparticle detection using six resistors in the series–parallel combination sensor SP6 (a) and experimental magnetic hysteresis loop of Fe_3O_4-chitosan magnetic nanoparticles (b; see also Ref. 19). The inset of (b) shows the region of the small field range.

due to the increase in H_d from the connections. As a result, the potential energy of the demagnetization field tends to weaken the magnetic order inside the magnetic bar and thus reduces the MR ratio in comparison with the Cu-connection sample. Additionally, the lower MR ratio could be attributed to the magnetic connector contribution, in which magnetic moments tend to align along the supplied current when magnetization reversal takes place. These segments contribute an MR ratio opposite to the magnetic bar in which the magnetic moments tend to align perpendicular to the current (Fig. 4, left).

To further strengthen the uniaxial magnetic anisotropy of the NiFe film, 5-nm-thick, bar-shaped permalloy strips with 150-μm width and 4-mm

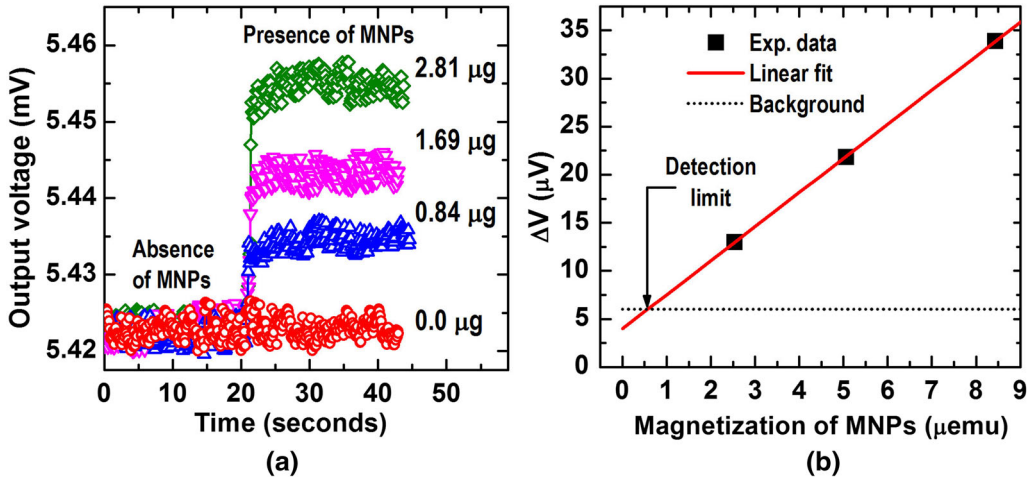

Fig. 9. Sensor output voltage response in the absence and the presence of different amounts of Fe3O4-chitosan MNPs (a) and dependence of signal change on magnetization of the MNPs (b).

length were designed. By using these dimensions, the in-plane aspect ratio of 26.67 should support in-plane magnetic shape anisotropy directed along the length of the bars.[2,15] However, since the volume of the strip was very small (about 3×10^{-9} cm^3), the maximum signal was approximately 2.3 μemu, which is close to the resolution of the vibrating sample magnetometer (VSM) used for the magnetization measurement. The output voltage response as well as magnetic sensitivity of the AMR Wheatstone bridge sensor is expected to be further enhanced by increasing the number of resistor NiFe strips connected in series in each bridge arm (Fig. 2b and c). Such a design would increase the $\Delta R/R$ contribution and thus the output voltage response according to Eq. 1. Figure 6 displays the voltage output response measured in sensors S1, S3 and S5 with one, three and five resistor strips connected in series, respectively. The results show that the maximum voltage signal indeed increases from 0.8 mV for S1 to 1.91 mV for S3 and to 2.85 mV for S5 for a current of 0.1 mA (Fig. 6a). These values are double when the current is increased to 0.2 mA (Fig. 6b). As a result of the increasing voltage signal, the magnetic field derivative dV/dH increases from 0.21 mV to 0.68 to 1.08 mV/Oe at a current of 0.1 mA corresponding to the sensors with one, three and five resistor strips, respectively (see also in Fig. 6c and Table I). Also, the coercivity decreases from 3.51 Oe to 2.14 Oe and 0.94 Oe corresponding to sensor S1, S3 and S5, respectively. Due to the high remanent magnetization of the NiFe film as shown in Fig. 3b, the decrease of coercive field could be attributed to the demagnetizing field contribution that builds up from the surrounding NiFe resistor elements.[16] Although the increase of current supplied supports further enhancement of the output voltage response,[2] this also causes increase of the noise background (inset Fig. 6b). This can be attributed to a higher number of resistors and thus more Johnson thermal noise caused by the increase of intrinsic resistance, as measured and listed Table I. The magnetic field sensitivity S_H is given by:

$$S_H = \frac{1}{V_{in}}\frac{dV}{dH} = \frac{1}{iR}\frac{dV}{dH}. \quad (5)$$

The calculated S_H values listed in Table I show that there is almost no change in the sensitivity of the sensor when increasing the number of resistors in series. This further improves the limitation of the AMR bridge sensor in the series connection approach (Fig. 7).

To reduce the thermal noise effect as well as the magnetic coercivity, and further enhance the AMR ratio by reducing the intrinsic resistance of Wheatstone bridge, a sensor made of six resistors connected in a series–parallel combination circuit (SP6) was investigated (Fig. 2d). Indeed, the SP6 resistance is about 1.8 kΩ, which is 50% of the S3 resistance (3.6 kΩ). The output voltage, the magnetic field derivative of the voltage, and the magnetic sensitivity are 1.5, 2.6 and 1.72 times higher than those of the simplest sensor S1, respectively (see Fig. 8 and Table I). In particular, a much lower coercivity of about 1.7 Oe is found in sensor SP6 in comparison with sensors S1 and S3, which once again supports our hypothesis of the demagnetizing field contribution. To improve the signal-to-noise ratio (SNR) and magnetic sensitivity for realizable sensor applications[17,18] such as biosensors, this combined connected configuration would yield an optimal design for an AMR Wheatstone bridge sensor.

Detection of Magnetic Nanoparticles

For biosensor applications, the series–parallel combination sensor SP6 was considered to be optimal for the detection of magnetic nanoparticles (MNPs). The sensor was packaged by making a

plastic well directly on the surface of the sensor at a sensing resistor arm (see in Fig. 8a). This aims to exactly localize the MNPs only on the sensing area. In this measurement, fluid suspensions of superparamagnetic Fe_3O_4-chitosan MNPs (50 nm) with various concentrations were dropped directly on the well using a micropipette. The MNPs were magnetized perpendicularly to the sensor surface using a magnetic field strength of about 100 Oe created by a permanent magnet placed close to the sensor. From the measured magnetization data shown in Fig. 8b, the MNPs exhibit magnetization as small as 3 emu/g at a magnetic field of 100 Oe.[19] As described in our previous section, this sensor is sensitive to the in-plane component of the stray field generated from MNPs, defined with orange lines in the inset of Fig. 8a (upper left). The entire system was placed between Helmholtz coils with a bias magnetic field of about 1.7 Oe applied in-plane, perpendicular to the pinned direction to maintain the highest sensor sensitivity. In Fig. 9a, the output voltage with a supplied current of 0.1 mA is plotted as different amounts of MNP samples are added to the sensor well facing the sensing area.[2] In the absence of MNPs, the average background noise of the sensor was estimated to be about 6 μV. In the presence of samples, the response of the sensor increases, reaching larger values as the amount of MNPs increases. The sensor's signal change is plotted in Fig. 9a as a function of the magnetization of MNP samples (Fig. 8b) and shows a perfect linear dependence on the calculated magnetic moment of MNPs. The detection limit is defined as the point where the sensor's signal change in the presence of MNPs must be higher than the background noise. This value extracted from Fig. 9b is not less than 0.56 μemu, which is several times more sensitive than that reported recently for an AMR sensor in a series connection,[2,20] and almost two orders of magnitude lower than that of 18.7 μemu reported by Volmer et al. in the permalloy-based PHE sensor disks.[21] This value is comparable with that of the sensor based on the magnetoelectric effect.[19] As a way to compare different sensor sizes or MNP amount, the detection limit of magnetic moment per sensor area, estimated to be 194×10^{-15} emu/μm^2, may be used. This value is nearly 5 times better than the calculated value of 920×10^{-15} emu/μm^2 in giant magnetoresistive (GMR) biosensors reported by Wang et al.[22] and comparable with that value of 72.5×10^{-15} emu/μm^2 in the sensor reported by Lin et al.[23]

CONCLUSION

The output voltage response of the AMR Wheatstone bridge sensor was enhanced by increasing the number of resistor NiFe strips connected in series in each bridge arm as a result of the increase in intrinsic resistance. The disadvantage of this connection is that while the magnetic sensitivity of around 1.8 mV/V/Oe remains almost unchanged, the Johnson thermal noise contribution is increased when increasing the number of strips. However, the magnetic coercive field was remarkably reduced thanks to the presence of demagnetization fields that built up in the surroundings of resistor elements. Combining the reduction in magnetic coercive field, increase in magnetic sensitivity and the lowering of Johnson thermal noise, an improved SNR for realizable sensor applications, such as bio-sensors, has been achieved in the series–parallel combination configuration. By using this sensor, Fe_3O_4-chitosan MNPs with a diameter of 50 nm, the detection limit of magnetic moments was estimated to be about 0.56 μemu in solution. Considering the high magnetic moment resolution compared to the spin-valve-based GMR sensor, and very simple construction and production process, this sensor is effective in a wide range of low-cost biosensing applications.

ACKNOWLEDGMENTS

This work was supported by Vietnam National University, Hanoi, under the granted research Project Nos. QG 16.26 and QG 16.28.

REFERENCES

1. M.J. Haji-Sheikh and Y. Yoo, *J. Int. Intell. Syst. Technol. Appl.* 3, 95 (2007).
2. L.K. Quynh, B.D. Tu, D.X. Dang, D.Q. Viet, L.T. Hien, D.T.H. Giang, and N.H. Duc, *J. Sci. Adv. Mater. Dev.* 1, 98 (2016).
3. D. Henriksen, B.T. Dealslet, D.H. Skieller, K.H. Lee, F. Okkels, and M.F. Hansen, *Appl. Phys. Lett.* 97, 013507 (2010).
4. P. Mlejnek, M. Vopálenský, and P. Ripka, *Sens. Actuators A* 141, 649 (2008).
5. A. Persson, R.S. Bejhed, H. Nguyen, K. Gunnarsson, B.T. Dalslet, and F.W. Østerberg, *Sens. Actuators A* 171, 212 (2011).
6. A.D. Henriksen, B.T. Dalslet, D.H. Skieller, K.H. Lee, F. Okkels, and M.F. Hansen, *Appl. Phys. Lett.* 97, 013507 (2010).
7. M. Doescher, Magnetoresistive sensor having a strip-shaped conductor and a screening strip, United States Patent (2006).
8. J.B. Johnson, *Nature* 20, 119 (1927).
9. Y.-C. Liang, L. Chang, W. Qiu, A.G. Kolhatkar, B. Vu, K. Kourentzi, T. Randall Lee, Y. Zu, R. Willson, and D. Litvinov, *Sensors* 17, 1296 (2017).
10. G. Li, S. Sun, R.J. Wilson, R.L. White, N. Pourmand, and S.X. Wang, *Sens. Actuators A* 126, 98 (2006).
11. W. Wang, Y. Wang, T. Liang, Y. Feng, T. Klein, and J.-P. Wang, *Sci. Rep.* 4, 5716 (2014).
12. S.X. Wang and G. Li, *IEEE Trans. Magn.* 44, 1687 (2008).
13. J. Devkota, C. Wang, A. Ruiz, S. Mohapatra, and P. Mukherjee, *J. Appl. Phys.* 113, 104701 (2013).
14. J. Devkota, G. Kokkinis, T. Berris, M. Jamalieh, S. Cardoso, F. Cardoso, H. Srikanth, M.H. Phan, and I. Giouroudi, *RSC Adv.* 5, 51169 (2015).
15. S. Ingvarsson, G. Xiao, S.S.P. Parkin, and W.J. Gallagher, *J. Magn. Magn. Mater.* 251, 202 (2002).
16. Y. Zhang, Z. Dong, W. Yu-Kun, Y. Yu-Li, H. Zhao-Cong, L. Chen, and Z. Ya, *Chin. Phys. B* 22, 056801 (2013).
17. M. Volmer and M. Avram, *Microelectron. Eng.* 108, 116 (2013).

18. B.D. Tu, T.Q. Hung, N.T. Thanh, T.M. Danh, N.H. Duc, and C. Kim, *J. Appl. Phys.* 104, 074701 (2008).
19. D.T.H. Giang, D.X. Dang, N.X. Toan, N.V. Tuan, A.T. Phung, and N.H. Duc, *Rev. Sci. Instrum.* 88, 015005 (2017).
20. L.T. Hien, L.K. Quynh, V.T. Huyen, B.D. Tu, N.T. Hien, D.M. Phuong, P.H. Nhung, D.T.H. Giang, and N.H. Duc, *Adv. Nat. Sci. Nanosci. Nanotechnol.* 7, 045006 (2016).
21. M. Volmer and M. Avram, *J. Magn. Magn. Mater.* 381, 481 (2015).
22. W. Wang, Y. Wang, T. Liang, Y. Feng, T. Klein, and J.-P. Wang, *Sci. Rep.* 4, 5716 (2014).
23. G. Lin, D. Makarov, M. Melzer, W. Si, C. Yanac, and O. Schmidt, *Lab Chip* 14, 4050 (2014).